Research Article GU J Sci 36(2): 675-691 (2023) DOI: 10.35378/gujs.1067707

Gazi University

Journal of Science

http://dergipark.gov.tr/gujs

Torque Capability Comparison of Induction and Interior Permanent Magnet Machines for Traction Applications

Tayfun GUNDOGDU*

Hakkari University, Faculty of Engineering, Department of Electrical and Electronic Engineering, 30000 Hakkari, Turkey

Highlights

- This paper focuses on performance comparison of induction and interior permanent magnet machines.
- A comprehensive literature review on electric vehicle applications is presented.
- The underlying causes of the induction machine producing more torque are exposed.
- Flux weakening capabilities and efficiency maps have been compared.

Article Info

Received: 03 Feb 2022
Accepted: 22 May 2022

Keywords

Induction machine
IPM machine
Torque capability
Toyota Prius 2010
Saliency

Abstract

This paper investigates the torque generating capabilities and performance comparison of induction machines (IM) and interior-permanent magnet (IPM) machines for electric vehicle (EV) traction applications. Electromagnetic performance characteristics, such as torque, torque ripple, air-gap flux density, etc. are quantitatively compared by changing the level of electric loading. Other performance metrics such as saturation factor, power losses, efficiency, and so on, as well as the flux-weakening capability and efficiency map have also been compared. For calculations of the electromagnetic performance characteristics, 2D time-stepping finite element analysis (FEA) has been employed. It has been revealed that due to the reduction in torque components of IPM machine as a consequence of magnet demagnetization, it cannot generate toque as high as IM under overloading operating conditions. A thorough review of the literature on comparative studies on the electrical machines used in EV or Hybrid EV (HEV) applications is also included.

1. INTRODUCTION

The International Council on Clean Transportation oversees worldwide CO_2 emission regulations for new passenger vehicles, which are increasing each year to promote public health and prevent climate change [1]. Consequently, in order to enhance the eco-efficiency of the transportation, the emphasis on automobile electrification has grown significantly in the previous decade. Since electrical machines are at the core of electric vehicle (EV) propulsion systems, their improvement, along with power electronic and energy storage subsystems, has received a lot of attention. Interior-permanent magnet (IPM) rotor topologies are employed in the propulsion systems of the world's leading commercial hybrid electric vehicles (HEVs) and EVs, including Tesla/Model 3, Nissan/LEAF, Renault/Zoe, Toyota/Prius, Mitsubishi/Outlander, Hyundai/Kona, BMW/i3, Audi/e-tron, Kia/Niro, and many others. Alternatively, some other vehicles, such as Tesla (Model S), BMW (X5), GM (EV1), Renault (Kangoo), Chrysler (Durango), and several other vehicles use induction machines (IMs) [2-10]. Electrical machines designed for propulsion applications should have the following essential performance characteristics: high-starting torque, high-efficiency over a wide speed range, high-power and torque densities, low-torque ripple, high-reliability, and affordable cost [11,12].

The reason for the preference of IMs in the EV and HEV applications is their mature manufacturing technology, robustness, relatively low cost, good dynamic torque control performance, and simplicity. The joule losses and, as a result, the cooling equipment requirements increase due to the conductor bars on the rotor. When compared to IPM machines, this results in a lower overall efficiency. IPM machines, on the

* e-mail: tayfungundogdu@hakkari.edu.tr

other hand, benefit from the use of NdFeB permanent magnets (PMs), which provide high-torque, power, and also efficiency. Because of the superior characteristics of IPM machines, they are more popular than IMs in EV and HEV applications. The high cost of NdFeB PM, on the other hand, has a serious impact on the popularity of IPM machines [6].

A number of research papers on the comparison of electrical traction machines used in EV and HEV applications have been published in the literature. These studies compare IM with a various of different machine technologies including IPM machines with different rotor topologies, i.e. U-V-W-shapes, various PM layers, and etc. (IPM 2), IPM machines designed with one of the rotor topologies given in IPM 2 (IPM 1), surface-mounted PM (SPM) machine, switched reluctance machine (SRM), synchronous reluctance machine (SnyRM), brushless DC (BLDC) machines, PM assisted SRM (PMaSRM), claw-pole (CP) machine [2-20]. Moreover, some of the studies have been investigated the design and drives of these traction machines [5,10-12] and [21-24]. Comparison studies and compared machine and drive technologies are summarized in Table 1.

Table 1. *Comparison studies on EV/HEV traction machines*

Machine Technology	***Reference***
IM	[3-8,11-13,18]
IPM 1	[4-8,13,18,20,24]
IPM 2	[3,9-12,14-17,19]
SPM	[10-13,15,20]
SRM	[5,6,8,11-13]
SnyRM	[8,11,12]
BLDC	[5,11,12]
PMaSRM	[5,11,12]
CP	[5]
Drive	[5,10-12,21-24]

A comparative study on four traction machines, namely; direct current (DC) machine, cage-rotor IM, surface-mounted PM (SPM) machine, and switched reluctance machine (SRM), has been conducted in [2]. Efficiency, power and torque densities, durability, controllability, technological maturity, and cost have all been considered when comparing these machines. The IM, among the machines evaluated, was found to better meet the key requirements of HEV propulsion. In [3], cage-rotor IM and IPM machines with various rotor configurations, i.e., U-V-W-shapes, various PM layers, and so on, were compared on the basis of torque-density, power factor, efficiency, and saturation levels, as well as the basic methods for design and analysis of these machines. One of the study's primary results is that, while having a high-torque density, the IM design is particularly susceptible to saturation, making it a potential alternative to IPM machines. [11,12] consider relative merits and some important major characteristics, including drive properties. It has been emphasized that the squirrel-cage IMs have mature manufacturing technology and can provide the needed drive characteristics. However, PM machines offer higher efficiency and torque density. In [3-8,11-13,18], IM has been compared with IPM machines in terms of torque and power density, power losses, material costs, etc. However, in none of these studies, torque capabilities have been investigated. As a result, the primary purpose of this study is to fill that gap, and the second purpose is to establish which machine is capable of generating the most torque and discuss the underlying causes.

This study is concerned with the design and quantitative comparison of electromagnetic performance characteristics, particularly the electromagnetic torque generating capabilities of IM and IPM machines operated under various electric loadings. The IPM machine was simply adopted for the Toyota Prius 2010, and the IM was designed with the same geometric and operating specifications, as well as winding arrangement with 5-slot pitch conventional single-layer windings, for a fair comparison. The obtained comparison findings between IM and IPM are presented and discussed, including flux linkage and locus, induced voltage, back-EMF, current angle, time-averaged torque, torque ripple, saturation factor, power losses, flux-weakening capabilities, and efficiency maps.

2. DESIGN OF IM AND IPM MACHINE

The variation of IM and IPM machine performance characteristics is analysed using the 2D finite element method (FEM) for various electric loading operations. In order to investigate the torque generating capabilities, the electric loading level has been varied from half to six times of the rated current value.

Table 2. *Design and operating specifications*

Parameters	Prius IPM	IM
Peak rated current (A)	250	250
Synchronous speed (rpm)	1500	1500
Number of stator slots	48	48
PM/Rotor slot number	16	44
Number of poles	8	8
Stator outer diameter (mm)	264	264
Stator inner diameter (mm)	161.9	195
Air-gap length (mm)	0.73	0.73
Stator slot opening width (mm)	1.88	1.88
Stator slot width (mm)	7.55	8.77
Stator slot height (mm)	30.9	13.85
Rotor slot opening width (mm)	–	1
Rotor slot width (mm)	–	9.29
Rotor slot height (mm)	–	15.2
PM dimensions (mm)	49.3 × 17.88	–
Number of turns per slot	11	7
Number of turns per phase	88	56
Slot filling factor	0.465	0.465
Stator phase resistance (@20°C) (Ω)	0.077	0.08
Core material	M270_35	M270_35
PM/Cage material	N35UH	Copper

The same operating conditions and geometrical specifications, as shown in Table 2, are adopted for a fair comparison and to obtain comparable results. In addition, the core material properties of the M270_35 is shown in Figure 1. Moreover, the magnetic specifications of the N35UM material are given as follows. The relative permeability (μ) 1.09978 and coercivity (H_c):-890000 A/m. Toyota Prius 2010 IPM is directly adopted by using the optimized specifications [25] and IM is optimized by using an analytical method given in [7]. 2-D cross-sectional views of the IPM machine and IM is illustrated in Figure 2. Very useful design guidelines for traction application of IMs and IPM machines are given in [11].

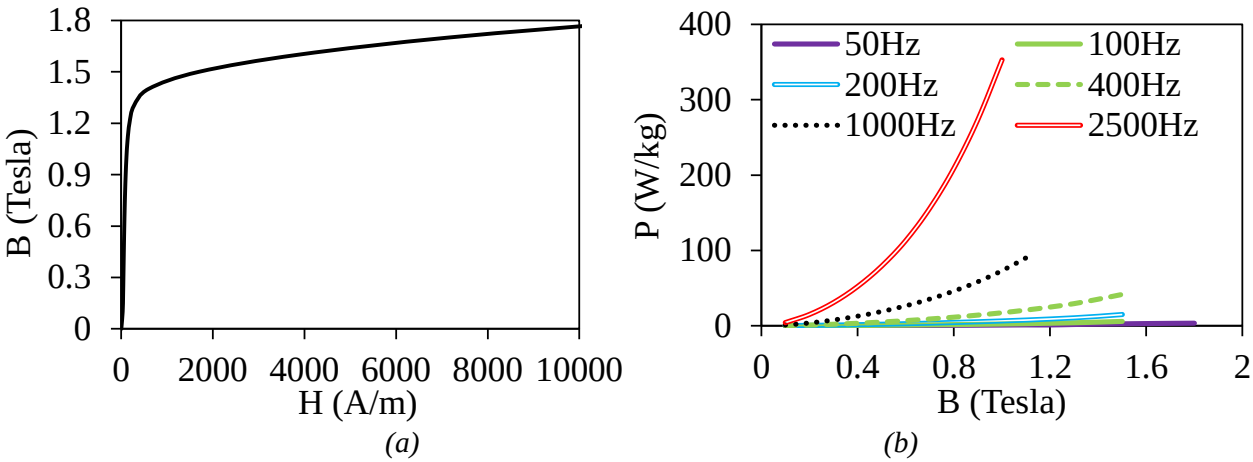

Figure 1. *M270_35 core material specifications: (a) BH Curve; (b) PB curve for various frequencies*

3. PERFORMANCE COMPARISON

The IPM machine and IM's performance characteristics are evaluated using a *dq*-axis reference frame, with the *d*-axis aligned with the rotor field [26]. Figure 3 illustrates the variation of the *dq*-axes currents with respect to current angle θ. θ is one of the vital parameters that should be determine firstly in order to operate the machine at maximum torque. This term has been determined by conducting parametric analyses for IPM machine and IM.

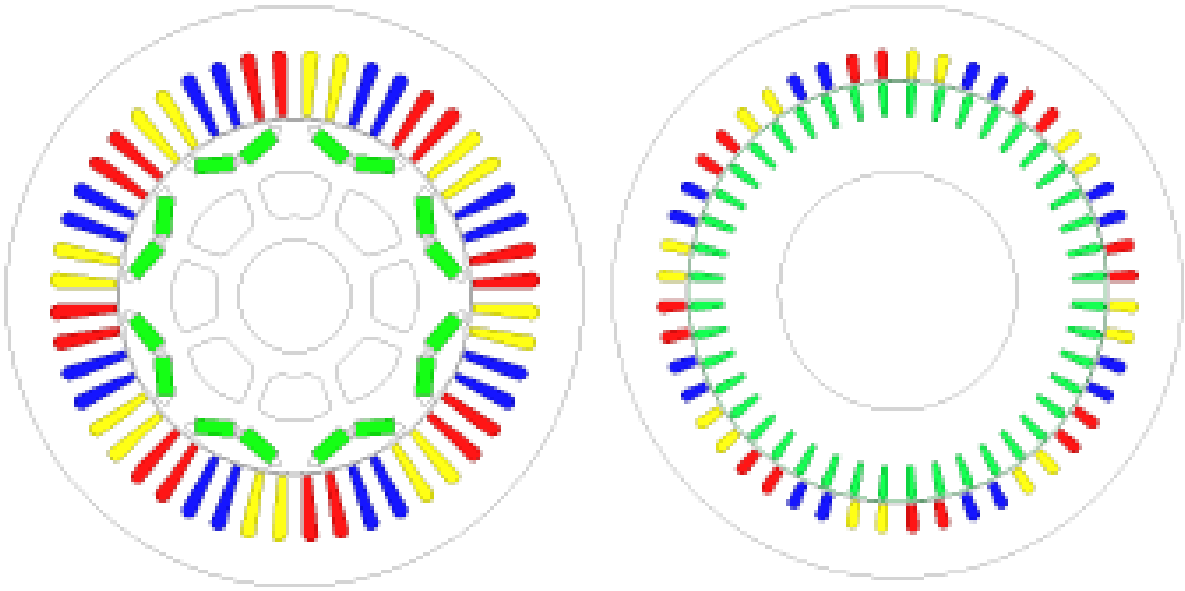

(a) *(b)*

Figure 2. *2D cross-sections: (a) Toyota Prius 2010 IPM machine; (b) IM*

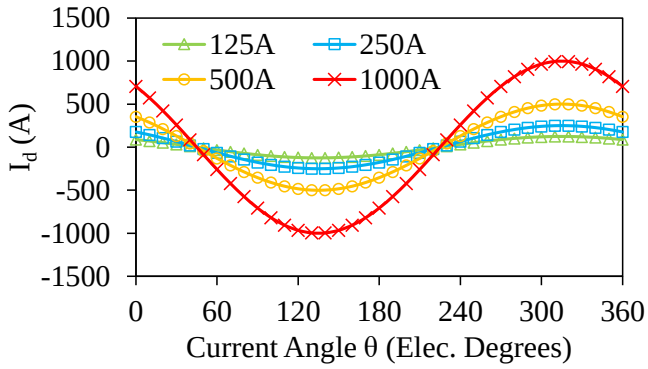

(a)

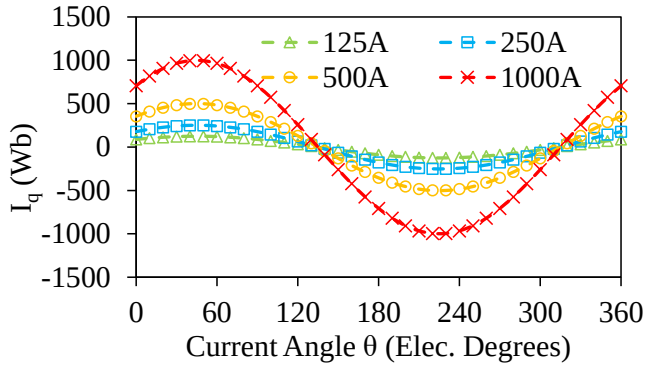

(b)

Figure 3. *Variation of current components with current angle: (a) I_d and (b) I_q*

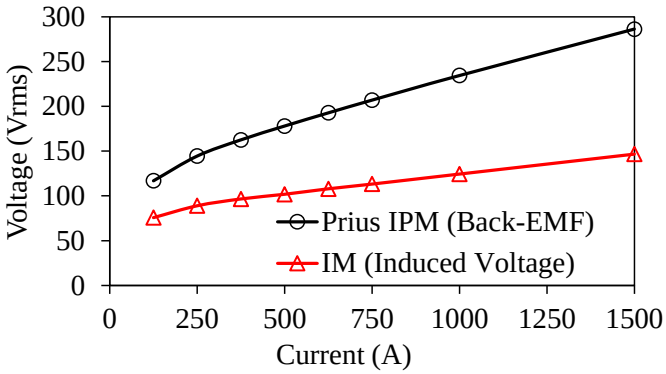

Figure 4*. Variation of Back EMF with respect to excitation current*

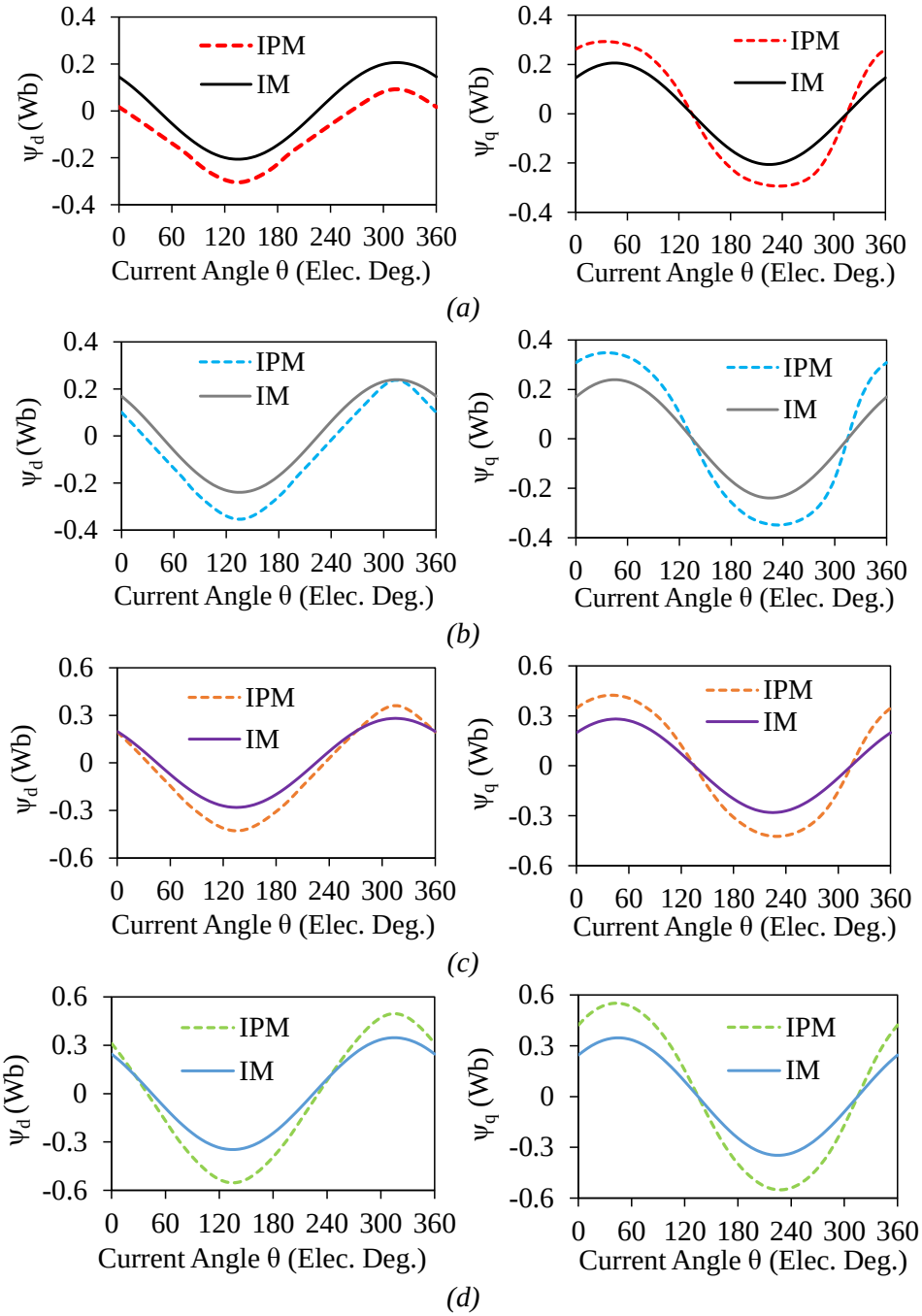

Figure 5. *Comparison of flux linkage component waveforms for IPM machine and IM for various excitation current: (a) 125A; (b) 250A; (c) 500A; (d) 1000A*

Figure 4 shows the influence of excitation current on the amplitude of the back-EMF. Whereas an IPM machine has many more turns per phase than an IM, the obtained rms value of the IPM machine's back-emf is substantially greater. Figure 5 depicts the fluctuation of the flux components with regard to θ for various current excitations.

While the amplitude of the *d*-axis flux ψ_d is smaller than that of the *q*-axis flux ψ_q for the IPM machine, these flux components are identical for IM, indicating that there is no saliency in the IM. Moreover, as for IPM machine, saliency ratio decreases while the excitation current increases. This phenomenon can be clearly seen in Figure 6.

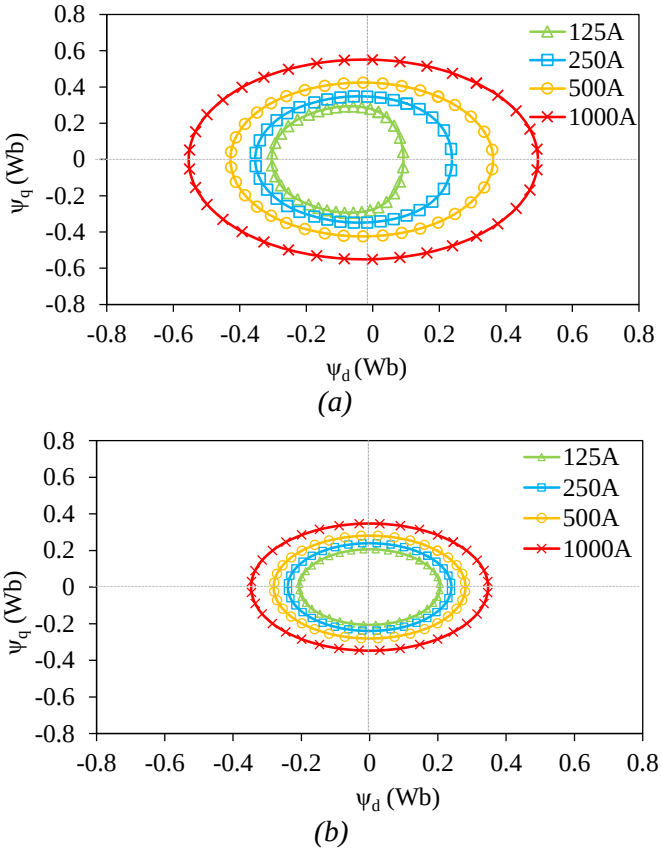

Figure 6. *Flux locus waveforms: (a) IPM machine; (b) IM*

As expressed in Equation (1), there are two variable components contributing the torque of PM machines. The first variable term in Equation (1) depends on the rotor excitation that is the PM flux ψ_{PM} depends on the properties of the PM material including size, maximum energy product BH_{max}, and etc. and the second term, known as reluctance torque, depends on the saliency of the rotor which is determined by inductance components L_q and L_d. The fixed term components are phase number m and pole pair number p

$$T_{em} = \frac{m}{2} p \left[\underbrace{\psi_{PM} I_q}_{\text{Excitation}} + \underbrace{(L_q - L_d) I_d I_q}_{\text{Reluctance}} \right]. \tag{1}$$

The IPM machines' electromagnetic torque may be estimated by modifying Equation (1) to include the flux components expressed in Equation (2). In addition, the electromagnetic torque of a squirrel-cage IM can be estimated via Equation (3), which is derived for stator flux-oriented IM drive [27,28]. In Equation (3), the superscript "*es*" denotes that the quantity is in the synchronous reference frame orientated to the stator flux

$$T_{em\_IPM} = \frac{3}{2} p (\psi_d I_q - \psi_q I_d) \tag{2}$$

$$T_{em\_IM} = \frac{3}{2} p\left(\psi_d^{es} I_q^{es}\right). \quad (3)$$

Calculated averaged electromagnetic torque varied with respect to current angle is illustrated in Figure 7. θ delivering the maximum torque in the motor operation mode has been determined as 270° and 0° electrical degrees for IPM machine and IM, respectively.

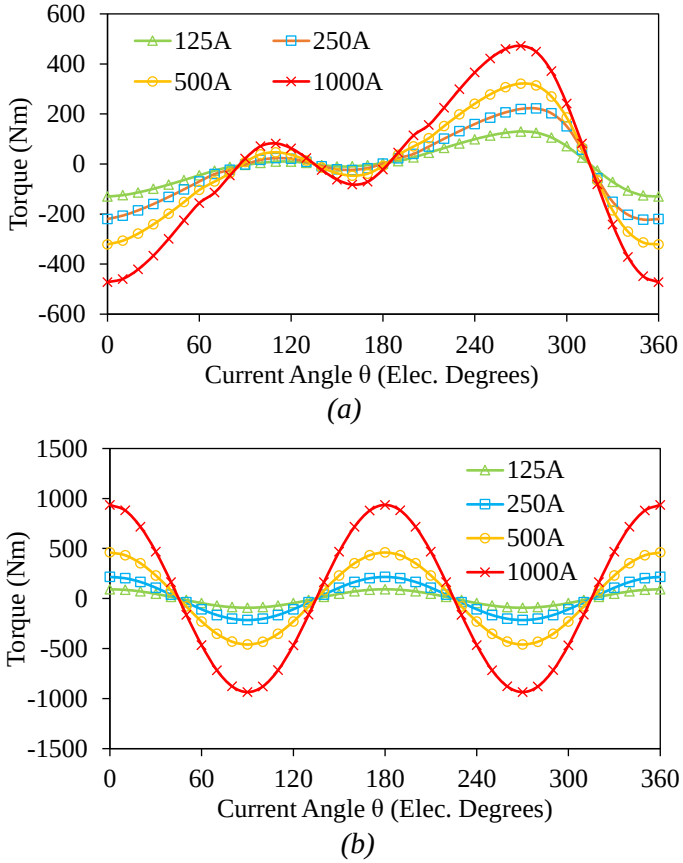

Figure 7. *Torque variations with respect to current angle: (a) IPM Machine; (b) IM*

Electromagnetic torque T capability and torque ripple ΔT percentage of the machines are illustrated in Figure 8. The rise in torque capabilities of the IM with current is substantially faster than that of the IPM machine. The figure also shows that the torque capability of the IPM machine is better for smaller electric load operations than the rated current (250A). However, when the electric load rises, the torque capability of the IM becomes significantly better than that of the IPM machine. In addition, since the average torque of IM increased significantly with electric load, its torque ripple decreased eventually after 500A. The torque ripple of the IPM machine, on the other hand, increases rapidly as the electric load increases.

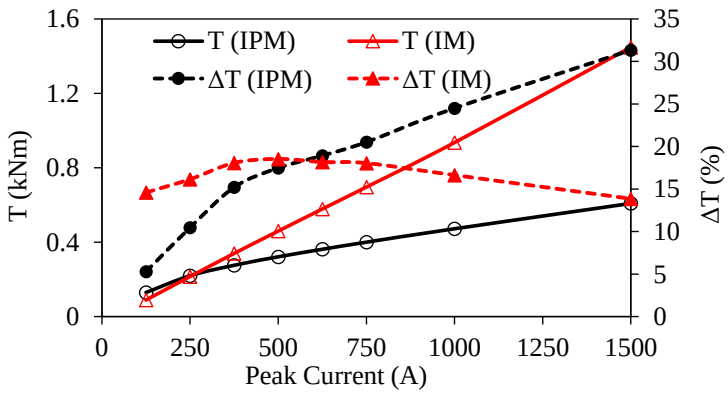

Figure 8. *Time-averaged torque and torque ripple percentage versus current*

As previously stated, the electromagnetic torque of PM machines is composed of two torque components: "PM" and "reluctance." The torque generated by PMs is proportional to the current, as shown in Equation (1), but the reluctance torque is proportional to the square of the current. Since the saliency ratio is decreased with increasing electric loading (see Figure 6), the reluctance torque component decreases. Besides, when the electric load increases, the effect of PMs becomes less prominent, as seen in Figures 9 and 10. Furthermore, the saturation generated by PMs may have an effect on the rise in torque of the IPM machine. The IPM machine, on the other hand, has PMs that have a constant flux magnitude. Even if the induced voltage is increased in the stator and the flux produced by the stator windings is increased with increasing excitation current, the flux produced by the PMs cannot be increased. Actually, as clearly seen in Figure 9, flux generated by PMs dramatically reduces as the excitation current increases. Flux line distributions for Toyota Prius IPM and IM is illustrated in Figure 10 for various current excitations. It can be seen that the flux produced by the PMs reduces as the current increases. In particular, in 1000A current excitation, almost no flux is produced by the PMs. The flux produced by the windings dominates the flux produced by the PMs. Therefore, since the flux density of the rotor core is way higher than the PM's flux density, quite a low flux can be produced by the PMs. Since the excitation and reluctance torque components of the IPM machine decreased dramatically as the excitation current increased, it could not generate torque as high as IM. It is also clear from the figures that the leakage flux is increasing with increased excitation current for both machines.

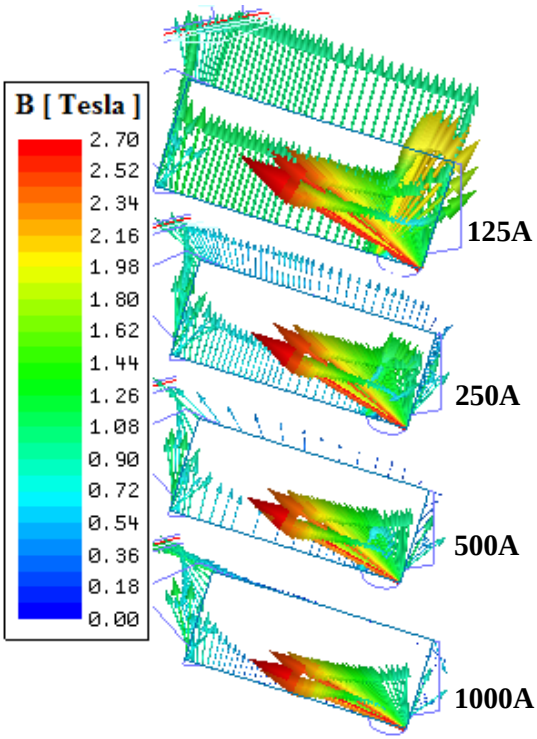

Figure 9. *Flux density vectors of PMs for various electric loadings*

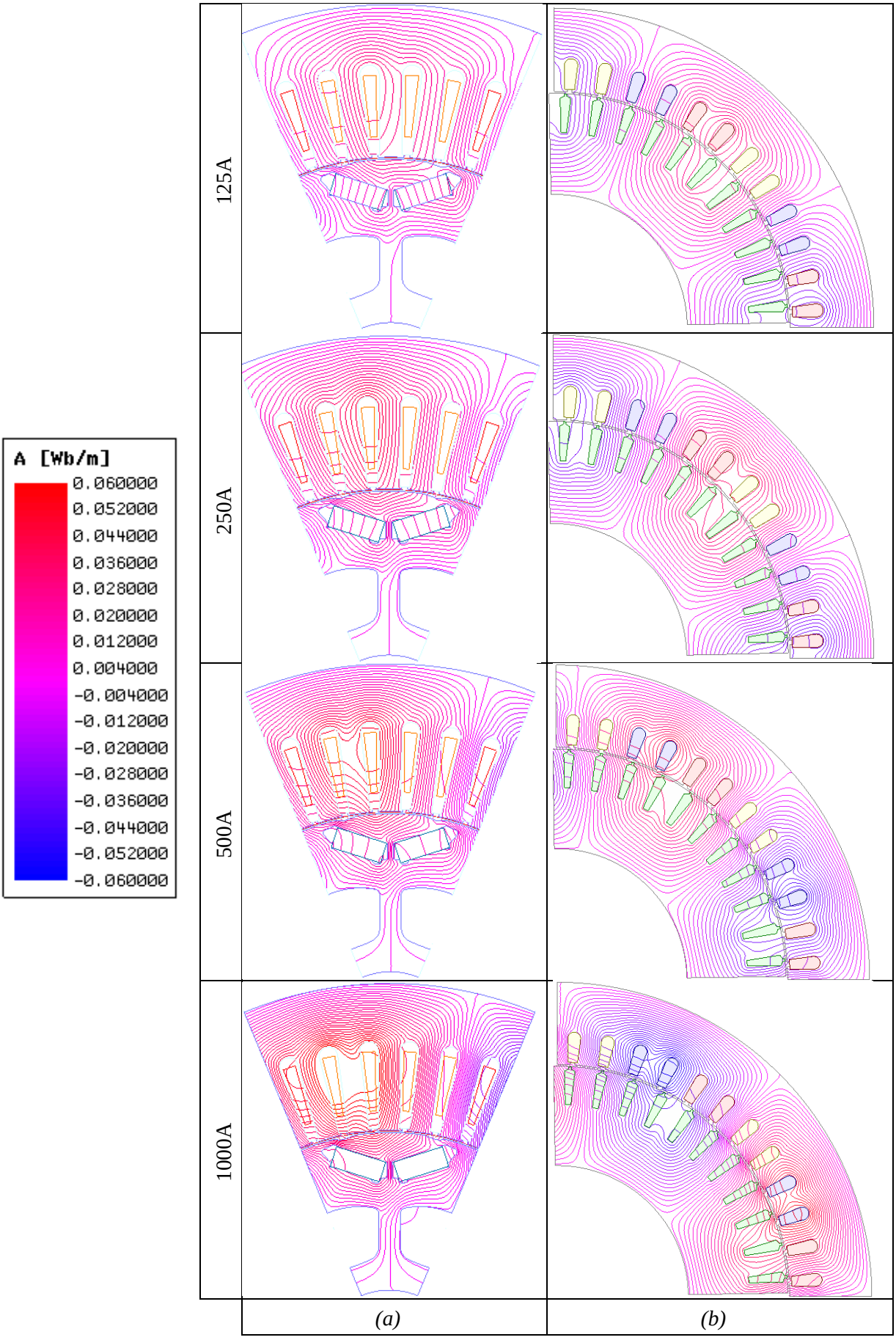

Figure 10. *Flux line distributions for various current excitations: (a) IPM machine and (b) IM*

For the IPM machine, the total flux is limited by PMs and saliency. However, for IM, with the increasing injected current, both the stator and rotor circuit's flux are increased. Because the rotor bar current will be increased by the increased excitation current. Therefore, since the total flux is increased, the obtained torque will also be increased. In theory, in comparison with PM machines, if the current density and heating issues are ignored, there is no torque limitation for the IMs. As for IM, the differential in magnetic fields between the stator and rotor, referred to as slip, rises as the electric load increases. Basically, the larger the electric load, the larger the slip as seen in Figure 11. To estimate the saturation levels of the machines, the saturation factor k_{sat_n} for both of the machines have been calculated by using Equation (4) and illustrated in Figure 12. The parameters of the saturation factor are magneto-motive force of stator MMF_{s_n}, rotor MMF_R, and, air-gap MMF_{g_n} or surface integrations of flux intensity of the same regions. As seen in Figure 12, saturation levels are quite similar, and they increase dramatically as electric loading increases.

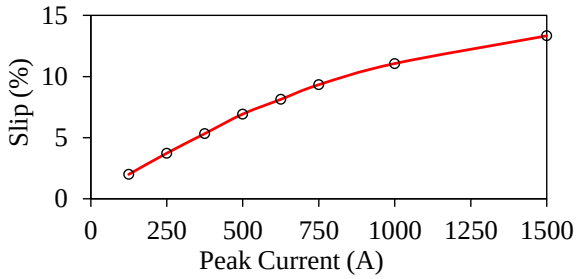

Figure 11. *Slip versus excitation current curve*

$$k_{sat_n} = 1 + \frac{MMF_{s_n} + MMF_{R_n}}{MMF_{g_n}} = 1 + \frac{H_{s_n} + H_{R_n}}{H_{g_n}} \tag{4}$$

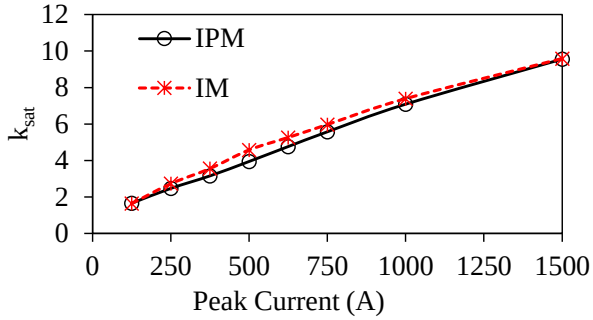

Figure 12. *Saturation factor versus excitation current*

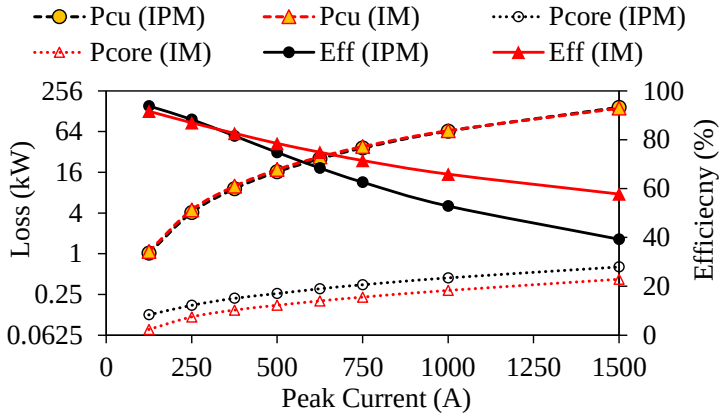

Figure 13. *Power losses and efficiency against excitation current*

The influence of electric loading on losses and efficiency has also been examined. The calculated copper loss P_{cu}, total core loss P_{core}, and efficiency percentage Eff are illustrated in Figure 13. Note that the copper

loss of IM $P_{cu}(IM)$ includes the sum of the stator and rotor bar copper losses. Furthermore, windage, friction, and stray load losses were considered to represent 1% of output power throughout the efficiency calculation [29]. Although copper losses are comparable, the core loss of the IPM machine is quite higher than that of the IM. Since the IPM machine has higher total machine loss and lower output power (see Figure 14) than the IM, the IPM machine's efficiency is noticeably lower than the IM under higher electric load operations.

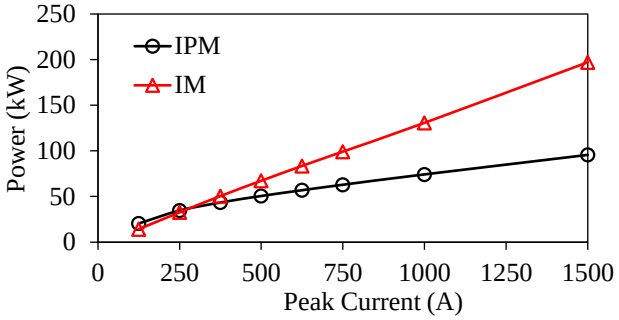

Figure 14. *Power versus excitation current curve*

4. FLUX-WEAKENING CAPABILITIES

The restricted excitation is one of the key limiting aspects of electrical motor drives. In the constant-torque area, the back-EMF increases with rotor speed until the inverter's voltage limit u_{max} is reached as expressed in Equation (5). The electrical motor is then put into flux-weakening mode. Because the voltage is restricted by the inverter's rating, the current (i_{max}) is also limited by the machine's rating (see Equation (6)). When phase current has a phase advance angle in comparison to the *q*-axis, the *d*-axis current i_d acts as a weakening current. Thus, the motors are controlled by maximum torque-per-ampere (MTPA) mode below corner speed and flux-weakening control mode above the corner speed [30]

$$V_d^2 + V_q^2 \leq u_{max}^2 \tag{5}$$

$$i_d^2 + i_q^2 \leq i_{max}^2. \tag{6}$$

The flux-weakening capabilities of induction and IPM machines have been calculated by employing *dq*-equivalent circuits and above mentioned MTPA control algorithm by considering the limited inverter ratings given in Equations (5) and (6). Figure 15 depicts a flow chart with a clear illustration of the flux-weakening computations.

As can be observed, the applied FW method combines numerical and analytical calculations. During the FEA stage, $[i_d]_{10x10}$ and $[i_q]_{10x10}$ matrices are injected into the phase windings of the NSW IPM to evaluate $[\lambda_d]_{10x10}$ and $[\lambda_q]_{10x10}$ flux linkage and $[P_{loss}]_{10x10}$ constraints/coefficient matrices. Following that, the generated matrices are utilized as inputs to the MATLAB® code developed in this work (see Figure 15), which calculates the output matrices, which include torque- and power-speed, power losses, and efficiency maps.

The flux-weakening capabilities have been calculated for various electric load operatings. The maximum inverter voltage is 650V, and this limit has not been exceeded in any electric load operation. Important design parameters and their influences on the flux-weakening characteristics of the IM are explained in [7,24]. Calculated torque/power-speed curves for various electric loading are illustrated in Figure 16. As seen in Figure 16(a), at 125A electric load operation, the IM's flux-weakening performance is inferior to that of the IPM machine. In certain speed regions, IM exhibits better flux-weakening performance at the rated electric loading (250A). However, output power drops dramatically at deep flux-weakening region (see Figure 16(b)). For 500A and 1000A electric load operations, the maximum torque and power/speed

characteristics of the IPM machine is considerably poorer than the IM especially at the constant torque region (see Figure 16(c, d)).

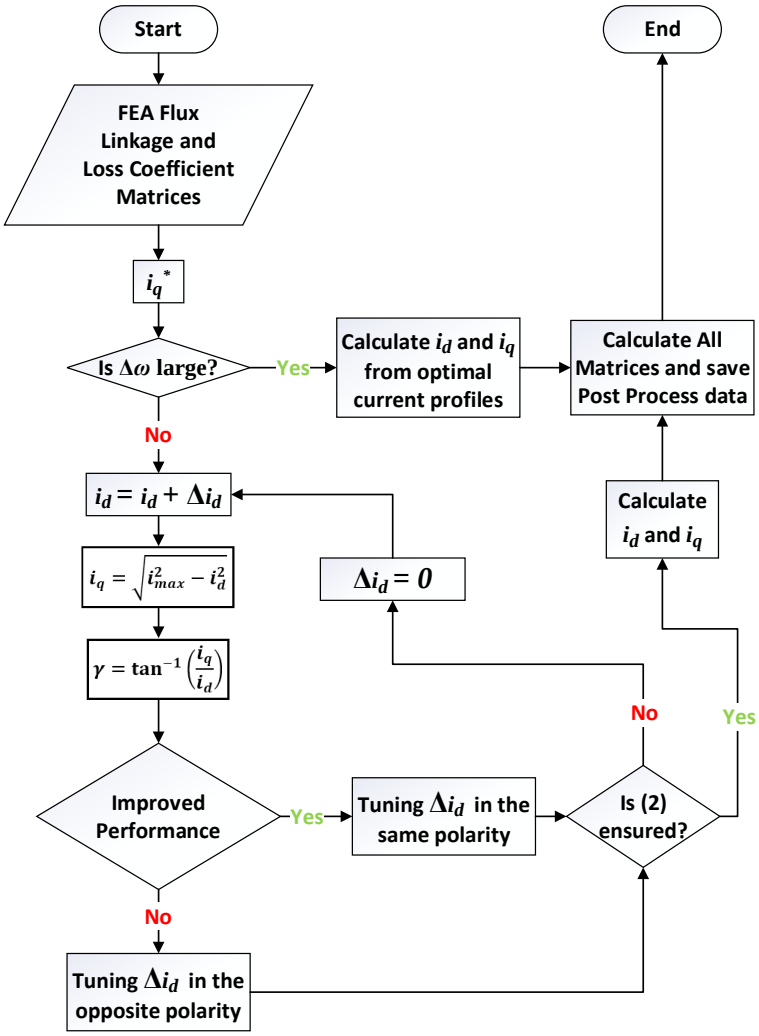

Figure 15. *Flow chart of the flux-weakening algorithm*

IPM machines' flux-weakening performances are affected by the saliency ratio and also PM material properties. Because the IPM machine has a lower torque capability under high electric loadings, its overall flux-weakening performance is lower than that of the IM under high electrical loadings. However, regardless of the electric loading level, the torque and power density of the IPM are clearly superior to the IM in the deep flux-weakening regions. Moreover, generally, the constant torque region of an IPM machine is slightly larger than the IM. Efficiency maps of the IPM machine and IM are calculated for the rated current excitation operation by using the expressions given between Equations (4) and (13). Note that all the terms, except for the mechanical loss coefficients k_{m1} and k_{m2} and p, are square matrixes obtained for a number of I_d and I_d excitations. R_{0_IPM} and R_{0_IM} are the phase resistances calculated at 20℃ for IPM machine and IM, respectively. In additional to stator copper loss, rotor bar copper loss, estimated by the square of bar current I_{bar} multiplied by bar resistance R_{bar}, is included for IM Equation (8). Total stator and rotor core loss can be calculated by using (9), where P_{hsy} is hysteresis loss, P_{exc} is excessive loss, P_{edd} is eddy current loss, f_1 is working frequency, and f_0 is the fundamental frequency. Mechanical P_{mech} and additional losses P_{add} including the friction, wind and stray load losses have also been taken into account. Output power P_{out} is calculated by (12), where ω_e is the angular frequency

$$P_{cu\_IPM} = \frac{3}{2} R_{0\_IPM}\left(I_d^2 + I_q^2\right) \tag{7}$$

$$P_{cu\_IM} = \frac{3}{2} R_{0\_IM}\left(I_d^2 + I_q^2\right) + I_{bar}^2 R_{bar} \tag{8}$$

$$P_{core} = P_{hsy}\frac{f_1}{f_0} + P_{exc}\left(\frac{f_1}{f_0}\right)^{1.5} + P_{edd}\left(\frac{f_1}{f_0}\right)^2 \tag{9}$$

$$P_{mech} = k_{m1} f_0 + k_{m2} f_0^2 \tag{10}$$

$$P_{add} = 0.01 P_{out} \tag{11}$$

$$P_{out} = \frac{T_{em}\omega_e}{p} \tag{12}$$

$$\eta = 100\frac{P_{out}}{P_{out} + P_{cu} + P_{core} + P_{mech} + P_{add}}. \tag{13}$$

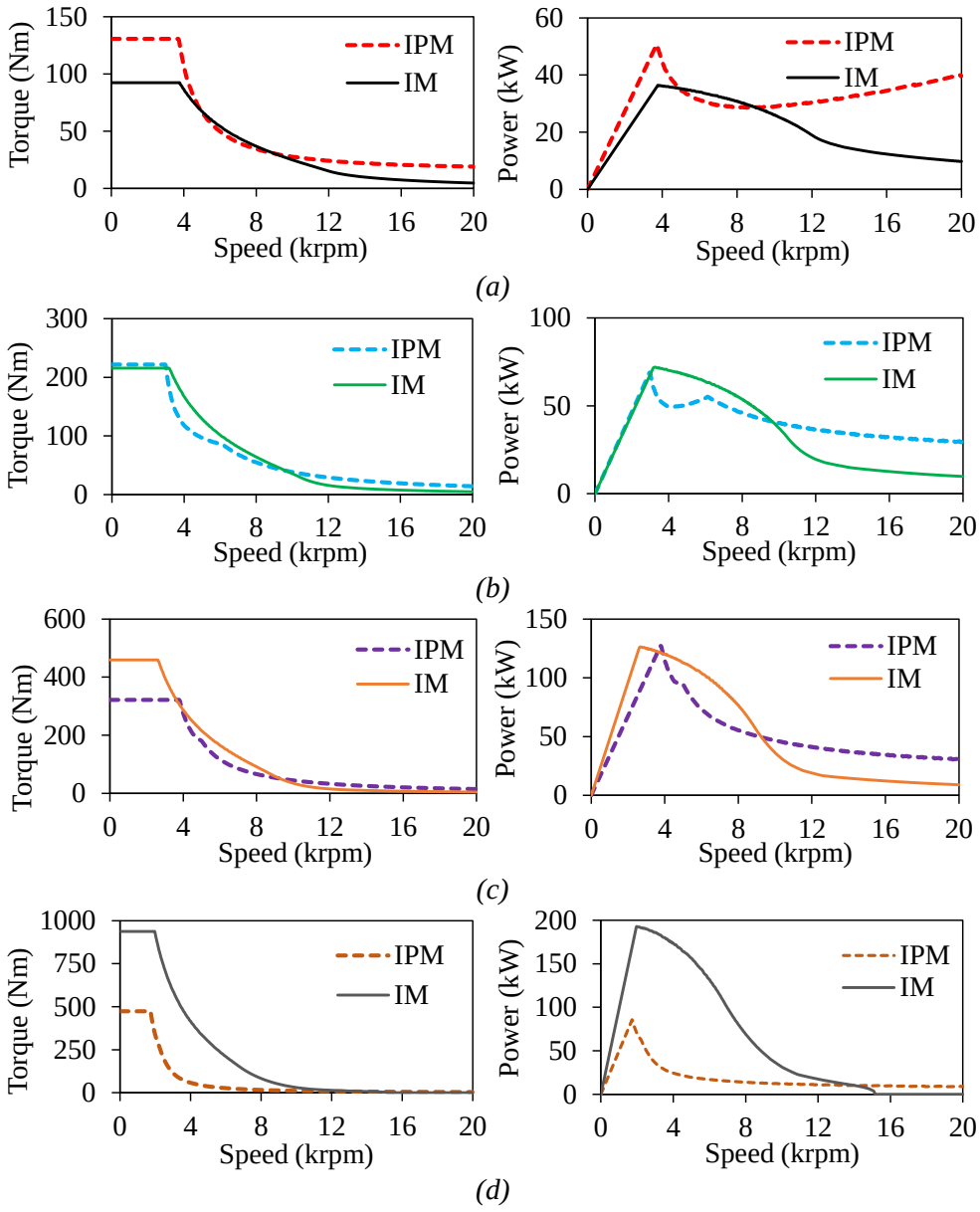

Figure 16. *Torque-Speed (left) and Torque-Power (right) characteristics for various current excitations: (a) 125A; (b) 250A; (c) 500A; (d) 1000A*

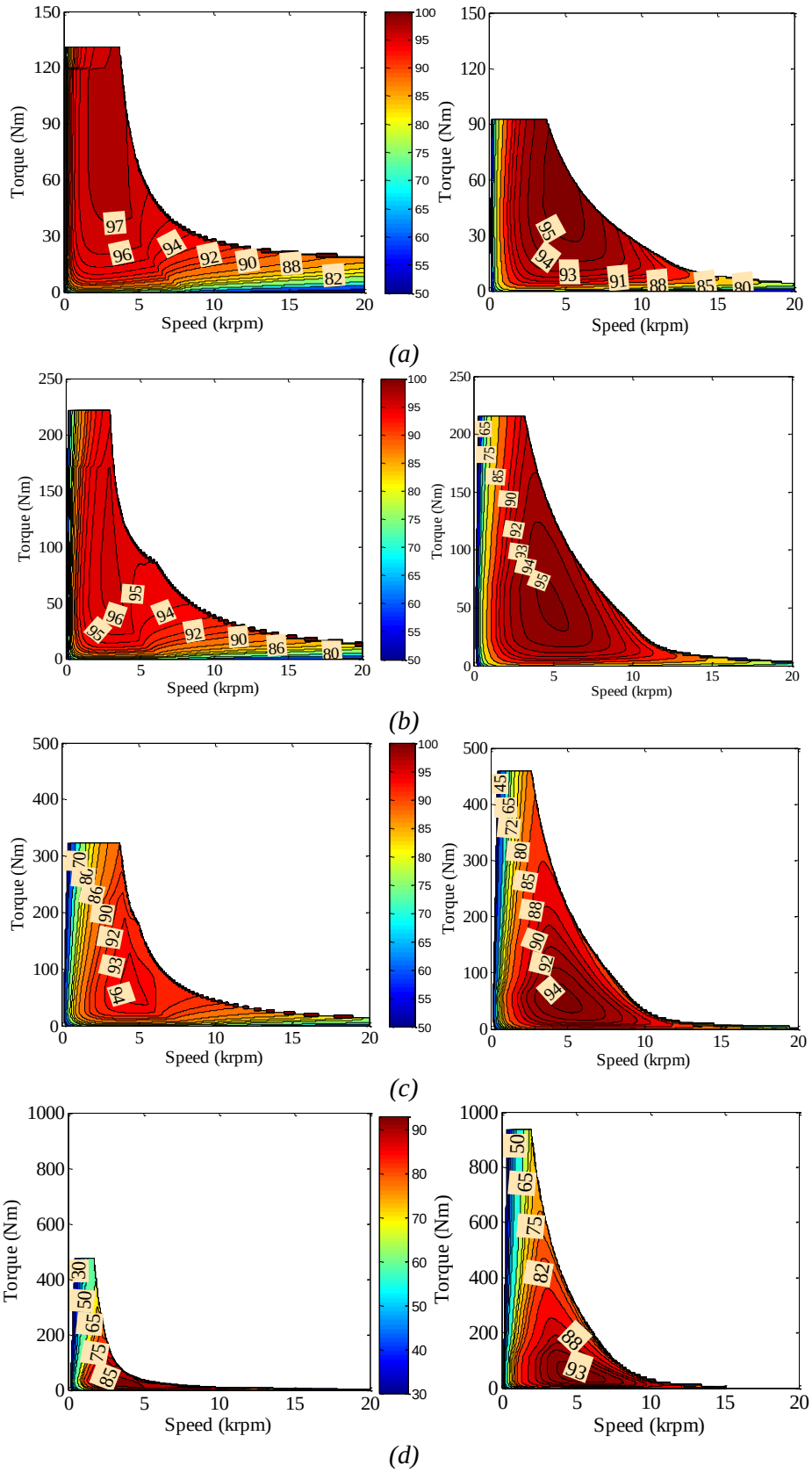

Figure 17. *Comparison of efficiency maps for IPM machine (left) and IM (right): (a) 125A; (b) 250A; (c) 500A; (d) 1000A*

Calculated efficiency maps for various electric loads are compared in Figure 17. The maximum efficiency difference between the IPM machine and the IM is summarized in Table 3. For both of the machines, the

highest efficiency has been obtained at 4 kpm and 6 krpm for the electric load between 125A and 500A. The IPM machine's power for 1000A is lower than half that of the IM. Therefore, the obtained maximum efficiency of the IPM machine is dramatically low, and it has been achieved between 3krpm and 5krpm. IM's overall efficiency is lower at the low electric loadings, and higher than that of the IPM machine at high electric load operating.

Table 3. *Comparison of Max. Efficiency of IPM Machine According to IM*

Electric Load	**125A**	**250A**	**500A**	**1000A**
η Difference (%)	+ 2.06	+ 1.04	0	− 9.41

5. CONCLUSION

The electromagnetic performance of the Toyota Prius 2010 IPM machine and IM, which are both designed with the identical outer diameter, stack length, winding topologies, and so on, has been quantitatively compared, with a focus on torque producing capabilities. The important findings are stated below:
The higher the electric loading;

- the torque rise of the IM is substantially faster than that of the IPM machine;
- the lower the torque ripple for IM while it is much higher for IPM machine;
- the lower the saliency and hence lower the reluctance torque component;
- the lower predominant PM effect and hence lower the excitation torque component;

    - ✓ the higher the slip percentage for IM;
    - ✓ the higher the saturation level for both of the IM and IPM machine;
    - ✓ the decrease of efficiency of IPM machine is much faster than the IM.

Furthermore, it has also been revealed that the torque capability of the IPM machine is better for low electric load operations (≤ 250A), while the torque capability of the IM is better for high electric load operations (> 250A). The IPM machine has a superior flux-weakening capability than IM at low electric loadings, whereas IM has a much superior capability at larger electric loadings. It is concluded that the IPM machine cannot produce torque as high as IM at high electric load operations due to a decrease in saliency ratio and PM flux density, which are the main torque-producing components of the IPM machine. As for future work, the driving cycle characteristics of an IM and an IPM machine will be compared, and strategies for improving the electric loading characteristics of IPM machines, such as increasing the saliency ratio and using various core and magnet materials, will be researched further.

CONFLICT OF INTEREST

No conflict of interest was declared by the author.

REFERENCES

[1] Diaz, S., Tietge, U., Mock, P., "CO_2 emissions from new passenger cars in the EU: Car manufacturers' performance in 2015", The International Council on Clean Transportation, (2016).

[2] Zeraoulia, M., Benbouzid, M. E. H., Diallo, D., "Electric motor drive selection issues for HEV propulsion systems: a comparative study", IEEE Transactions on Vehicular Technology, 55(6): 1756-1764, (2006).

[3] Dorrell, D. G., Knight, A.M., Evans L., Popescu, M., "Analysis and design techniques applied to hybrid vehicle drive machines — assessment of alternative IPM and induction motor topologies", IEEE Transactions on Industrial Electronics, 59(10): 3690-3699, (2012).

[4] Goss, J., Popescu M., Staton, D., "A comparison of an interior permanent magnet and copper rotor induction motor in a hybrid electric vehicle application", International Electric Machines and Drives Conference (IEMDC'13), Chicago, IL, 220-225, (2013).

[5] Boldea, I., Tutelea, L. N., Parsa, L., Dorrell, D., "Automotive electric propulsion systems with reduced or no permanent magnets: an overview", IEEE Transactions on Industrial Electronics, 61(10): 5696-5711, (2014).

[6] Yang, Z., Shang, F., Brown, I. P., Krishnamurthy, M., "Comparative study of interior permanent magnet, induction, and switched reluctance motor drives for EV and HEV applications", IEEE Transactions on Transportation Electrification, 1(3): 245-254, (2015).

[7] Guan, Y., Zhu, Z. Q., Afinowi, I. A. A., Mipo, J. C., Farah, P., "Comparison between induction machine and interior permanent magnet machine for electric vehicle application", COMPEL: The International Journal for Computation and Mathematics in Electrical and Electronic Engineering, 35(2): 572-585, (2016).

[8] Li, K., Bouscayrol, A., Cui, S., Cheng, Y., "A hybrid modular cascade machines system for electric vehicles using induction machine and permanent magnet synchronous machine", IEEE Transactions on Vehicular Technology, 70(1): 273-281, (2021).

[9] Groschup, B., Nell, M., Pauli, F., Hameyer, K., "Characteristic thermal parameters in electric motors: comparison between induction- and permanent magnet excited machine", IEEE Transactions on Energy Conversion, 36(3): 2239-2248, (2021).

[10] El-Refaie, A. M., "Motors/generators for traction/propulsion applications: A review", IEEE Transactions on Vehicular Technology, 8(1): 90-99, (2013).

[11] Zhu, Z. Q., Howe, D., "Electrical machines and drives for electric, hybrid, and fuel cell vehicles", Proceedings of the IEEE, 95(4): 746-765, (2007).

[12] Zhu, Z. Q., Chan, C. C., "Electrical machine topologies and technologies for electric, hybrid, and fuel cell vehicles", IEEE Vehicle Power and Propulsion Conference, Harbin, 1-6, (2008).

[13] Jiang, Y., Krishnamurthy, M., "Performance evaluation of AC machines for propulsion in a range extended electric auto rickshaw", IEEE Transportation Electrification Conference & Expo (ITEC'12), Dearborn, MI, 1-6, (2012).

[14] Wu, S., Tian, L., Cui, S., "A comparative study of the interior permanent magnet electrical machine's rotor configurations for a single shaft hybrid electric bus", IEEE Vehicle Power and Propulsion Conference, Harbin, 1-4, (2008).

[15] Wang, A., Jia, Y., Soong, W. L., "Comparison of five topologies for an interior permanent-magnet machine for a hybrid electric vehicle", IEEE Transactions on Magnetics, 47(10): 3606-3609, (2011).

[16] Liu, X., Chen, H., Zhao, J., Belahcen, A., "Research on the performances and parameters of interior PMSM used for electric vehicles", IEEE Transactions on Industrial Electronics, 63(6): 3533-3545, (2016).

[17] Yamazaki, K., Kumagai, M., "Torque analysis of interior permanent-magnet synchronous motors by considering cross-magnetization: variation in torque components with permanent-magnet configurations", IEEE Transactions on Industrial Electronics, 61(7): 3192-3201, (2014).

[18] Bucherl, D., Nuscheler, R., Meyer, W., Herzog, H. G., "Comparison of electrical machine types in hybrid drive trains: Induction machine vs. permanent magnet synchronous machine", International Conference on Electrical Machines (ICEM'08), Vilamoura, 1-6, (2008).

[19] Yang, R., Schofield, N., Emadi, A., "Comparative study between interior and surface permanent magnet traction machine designs", IEEE Transportation Electrification Conference & Expo (ITEC'16), Dearborn, MI, 1-6, (2016).

[20] Pellegrino, G., Vagati, A., Guglielmi, P., Boazzo, B., "Performance comparison between surface-mounted and interior PM motor drives for Electric Vehicle Application", IEEE Transactions on Industrial Electronics, 59(2): 803-811, (2012).

[21] Piña, A. J., Xu, L., "Comparison of apparent power consumption in synchronous reluctance and induction motor under vector control", IEEE Transportation Electrification Conference & Expo (ITEC'15), Dearborn, MI, 1-6, (2015).

[22] Pellegrino, G., Vagati, A., Boazzo, B., Guglielmi, P., "Comparison of induction and PM synchronous motor drives for EV application including design examples", IEEE Transactions on Industry Applications, 48(6): 2322-2332, (2012).

[23] Chan, C. C., "The State of the Art of Electric, Hybrid, and Fuel Cell Vehicles", Proceedings of the IEEE, 95(4): 704-718, (2007).

[24] Guan, Y., Zhu, Z. Q., Afinowi, I., Mipo, J. C., "Influence of machine design parameters on flux-weakening performance of induction machine for electrical vehicle application", IET Electrical Systems in Transportation, 5(1): 43-52, (2015).

[25] Olszewski, M., "Evaluation of the 2010 Toyota Prius hybrid synergy drive system", Oak Ridge National Labs, U. S. Department of Energy, (2011).

[26] Vas, P., "Vector Control of AC Machines", Clarendon Press, Oxford, 124-130, (1990).

[27] Xu, X., Doncker, R., Novotny, D. W., "A stator flux oriented induction machine drive", Annual IEEE Power Electronics Specialists Conference, Kyoto, Japan, 2: 870-876, (1988).

[28] Seibel, B. J., Rowan, T. M., Kerkman, R. J., "Field-oriented control of an induction machine in the field-weakening region with DC-link and load disturbance rejection," IEEE Transactions on Industry Applications, 33(6): 1578-1584, (1997).

[29] Gundogdu, T., Zhu, Z. Q., Mipo, J. C., Farah, P., "Investigation of non-sinusoidal rotor bar current phenomenon in induction machines—Influence of slip and electric loading", International Conference on Electrical Machines (ICEM'16), Lausanne, 1: 419-425, (2016).

[30] Gundogdu, T., Komurgoz, G., "Influence of design parameters on flux-weakening performance of interior permanent magnet machines with novel semi-overlapping windings", IET Electric Power Applications, Lausanne, 14: 2547-2563, (2020).